

ARTICLE OPEN



Highly stable superparamagnetic iron oxide nanoparticles as functional draw solutes for osmotically driven water transport

Changwoo Kim¹, Junseok Lee¹, Daniel Schmucker² and John D. Fortner¹✉

In this work, we develop and demonstrate highly stable organic-coated engineered superparamagnetic iron oxide nanoparticles (IONPs), which provide effective osmotic pressure without aggregation, reverse diffusion, or membrane blocking (by nanoparticles) for osmotically driven membrane systems, considering both forward osmosis (FO) and pressure-retarded osmosis (PRO). For this, we synthesized highly water stable, monodisperse 12 nm IONPs with a rational series of water stabilizing surface coatings, including sodium dodecyl sulfate (SDS), cetyltrimethylammonium bromide (CTAB), and polyethylene glycol (PEG). We then compared the library of surface functionalized IONPs as draw solutes for osmotic pressure-driven membrane processes. As synthesized, surface (organic) coatings are compact, thin, and can have very similar surface charge as the membrane itself, which results in effective osmotic pressure in forward osmosis (FO) mode configuration. To increase the osmotic pressure further, on a per mass basis, we synthesized and demonstrated novel hollow IONPs with identical surface coatings. Finally, water flux was further enhanced for stable particle systems using an oscillating magnetic field, thus physically altering concentration gradients, as a function of particle magnetic properties.

npj Clean Water (2020)3:8; <https://doi.org/10.1038/s41545-020-0055-9>

INTRODUCTION

Pressure retarded osmosis (PRO) and forward osmosis (FO) have attracted considerable attention with regard to water treatment and energy-based applications, among others^{1,2}. For both PRO and FO processes, developing stable, ideal draw solutes remains a major challenge. To be effective, draw solutes should have high solubility/stability, be nontoxic, and not physically or chemically interact with membrane surfaces, minimizing sorption or blocking³. In addition, production and recovery costs of draw solutes should be relatively low for scaled applications. Finally, there should be no reverse diffusion (draw solute permeation into the feed solution), which causes loss of osmotic pressures and concentration polarization (CP)⁴.

Magnetic nanoparticles (MNPs) have been considered as advanced draw solutes as they can be magnetically separated/regenerated. Among MNPs, superparamagnetic iron oxide nanoparticles (IONPs) are promising candidates because of their relatively low cost⁵ and toxicity⁶. To date, previous studies have reported IONPs as draw solutes with organic surface coatings, including triethylene glycol^{7,8}, polyacrylic acid⁹, poly(sodium acrylate)¹⁰, poly(N-isopropylacrylamide)¹¹, polyglycerol¹², dextran¹³, citrate¹⁴, and poly(ethylene glycol)diacid¹⁵. These reports have been summarized in tabular form in the SI for comparison, including results from this work. Among these, a relatively small number of studies were evaluated for long operation times (>4 h), all of which observed significant flux decline (up to 50%) due to membrane blocking (from the draw side)^{10,13}. For the regeneration/recovery of IONPs, most studies also observed aggregation, which also contributes to flux decline^{8,12,16–18}. For all, IONPs aggregation and deposition on the surface of membrane (blocking) remains a critical challenge for effective, long term operation. Toward this end, development of extreme stable IONPs is critical for the practical application of IONPs as draw solutes.

Colloidal stability of IONPs depends on particle size, density, surface chemistry, and aqueous conditions. Engineered IONPs can be synthesized by several methods, including thermal decomposition^{19,20}, co-precipitation²¹, and microemulsion²². For synthesizing monodisperse IONPs with high colloidal stability regimes, thermal decomposition methods using nonpolar solvents is an extremely reproducible strategy for highly monodisperse suspensions with precise surface coatings²³. Taking advantage of these methods, here we prepared and characterized 12 nm IONPs with a series of water stabilizing surface coatings, including sodium dodecyl sulfate (SDS), cetyltrimethylammonium bromide (CTAB), and polyethylene glycol (PEG), as nano draw solutes. All draw solutes evaluated in this study were demonstrated to be highly colloidal stable due to size and repulsive forces (including steric and electrostatic), which prevents particle aggregation and membrane blocking (draw side). In addition, we increased the performance of nano draw solutes by hollowing out the NPs core structure, and applying oscillating magnetic field.

RESULTS AND DISCUSSION

Synthesis of superparamagnetic IONPs and HNPs

Highly monodisperse 12 nm IONPs were synthesized by thermal decomposition in the presence of oleic acid (OA)^{20,24}. As measured by TEM (Fig. 1a), IONP size was 12.3 ± 1.0 nm; a size distribution is presented in Fig. 2a. The crystalline structure of the synthesized IONPs matched magnetite, Fe₃O₄ (JCPDS Card # 190629), which has been previously reported by our group and others (Fig. 2b)^{20,24}. In addition, IONPs were effectively 'hollowed' via an acid etching technique using technical grade TOPO (Fig. 1b, termed HNPs)²⁵. The resulting IONPs and HNPs were highly monodisperse and stable in nonpolar solvent due to the resulting hydrophobic surface (of the outward oleic acid tail facing into the organic solvent)²⁶.

¹Department of Chemical and Environmental Engineering, Yale University, New Haven, CT 06520, USA. ²Department of Energy, Environmental, and Chemical Engineering, Washington University in St. Louis, St. Louis, MO 63130, USA. ✉email: john.fortner@yale.edu

Synthesized IONPs were systematically coated by both ligand encapsulation and exchange methods, allowing for phase-transfer into water^{9,23,27}. For this, SDS, with a negatively charged sulfate terminal group, and CTAB, with a positively charged methyl ammonium terminal group, were used as ligand encapsulation agents. PEG (MW = 5 K) with hydroxyl functional groups within the polymer chain was used as a ligand exchange agent. Concentrations of phase transferred IONPs were ca. 300–500 mg/L. To concentrate further (up to ca. 2000 mg/L), suspensions were placed under vacuum to slowly remove water. For all concentration processes, there was no loss/aggregation of IONPs due to its high stability. The hydrodynamic diameters (D_H) and zeta potentials of phase transferred IONPs and HNPs were analyzed by DLS at pH 7. As shown in Fig. 2c, d, the zeta potentials for SDS-coated IONPs (IONP@SDS), CTAB-coated IONPs (IONP@CTAB), PEG-coated IONPs (IONP@PEG), and SDS-coated HNPs (HNP@SDS) were -25.5 , 26.7 , -6.3 , and -35.1 mV, respectively. D_H values for IONP@SDS, IONP@CTAB, IONP@PEG, and HNP@SDS were 23.5, 24.6, 37.7, and 26.3 nm, respectively.

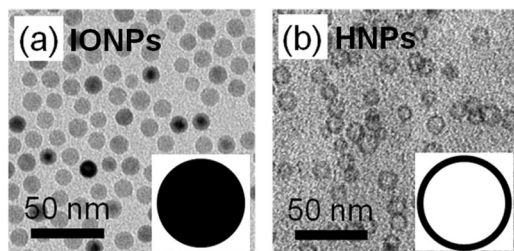


Fig. 1 TEM images of monodisperse NPs. (a) IONPs and (b) HNPs. Average diameter (12.3 ± 1.0 nm) of IONPs and HNPs was measured using Image-Pro 6.0 with over a thousand crystals counted.

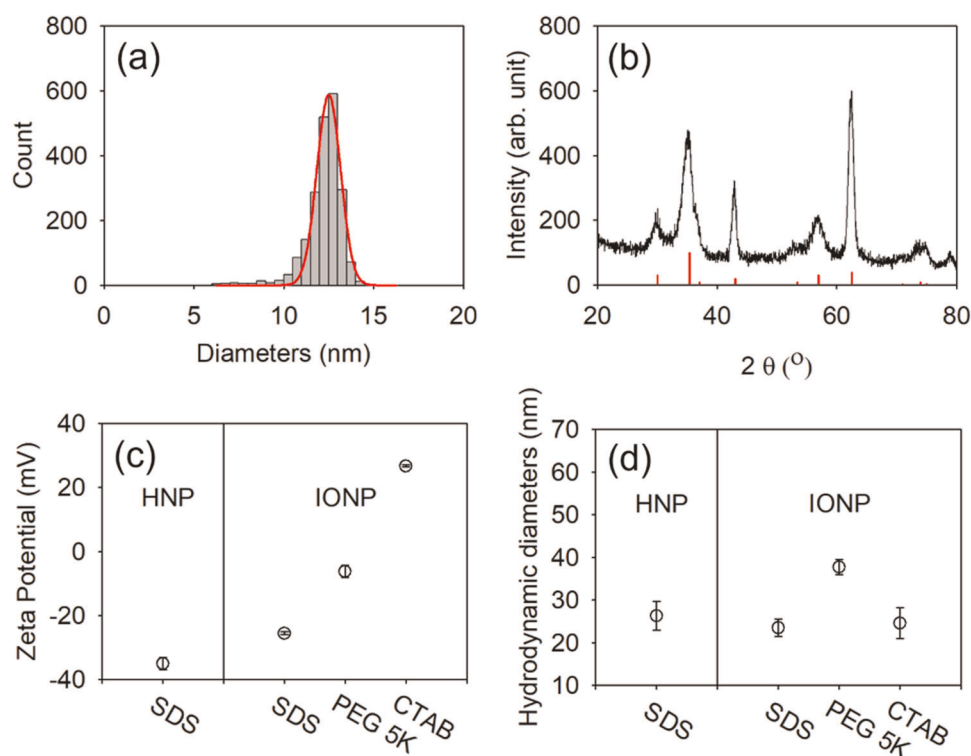


Fig. 2 Characterization of synthesized NPs. (a) Size distribution of synthesized IONPs. The average diameter and the standard deviation were 12.3 ± 1.0 nm. (b) X-ray diffraction (XRD) data of IONPs; diffraction patterns were well matched with magnetite (Fe_3O_4) crystalline structure (JCPDS Card # 190629, lower bars). (c) Zeta potentials and (d) hydrodynamic diameters of IONPs and HNPs coated with various surface stabilizers at pH 7.

Osmotic pressure driven membrane system

Concentration-dependent (450, 900, and 1800 ppm) draw solute tests were performed using IONP@SDS. Number concentrations of 450, 900, and 1800 ppm nano draw solution are 8.89×10^{16} , 1.78×10^{17} , and 3.35×10^{17} particles/L, which can produce theoretical osmotic pressure of 3.66, 7.32, and 14.64 Pa, respectively, based on the van't Hoff equation. The water fluxes were 0.19, 0.42, and 0.58 $\text{L}/\text{m}^2\cdot\text{h}$ for 450, 900, and 1800 ppm, respectively, in FO mode and 0.42, 0.60, and 1.16 $\text{L}/\text{m}^2\cdot\text{h}$ for 450, 900, and 1,800 ppm, respectively, in PRO mode (Fig. 3). As expected, when the particle concentration increased, the water flux increases, as particle concentration and osmotic pressure have a linear Van't Hoff based relationship. As shown by others, membrane blocking by nano draw solute (from draw side) is still critical issue need to be overcome (notable previous studies are summarized in Supplementary Table 1). Here, the increase in draw solution volume was approximately linear as a function of time, which also indicates minimal blocking. We hypothesize that the organic coating plays a significant role in NP draw solutes' behavior, as steric repulsion prevents NP aggregation and membrane adsorption^{28,29}. In addition, synthesized NPs are too large to pass through/into the membrane (via size exclusion). This fact was confirmed by measuring iron concentration of the feed solution after the experiments using ICP-OES. Over the tested concentration ranges, internal concentration polarization (ICP) has more influence on osmotic gradient than external concentration polarization (ECP) (i.e., flux of PRO mode is higher than that of FO mode). Both ICP and ECP profiles are presented in Supplementary Fig. 1. This is due to physical properties of the membrane support layer, such as the thickness, porosity, and tortuosity, as they relate to hindered transport/diffusion of draw solutes as discussed by others³⁰.

For optimized organic coated IONPs, the thickness and surface charge of the organic coating need to be considered. Organic

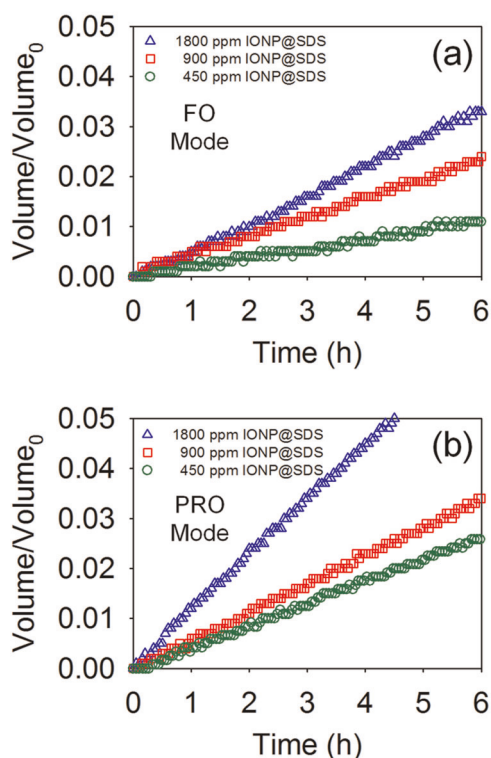


Fig. 3 Draw solute performances of synthesized NPs in osmotic pressure driven membrane processes (FO and PRO modes). Water fluxes were measured by time dependent total volume increase (V/V_0) with 0.95 cm^2 of effective membrane surface area (water flux = Increased volume/(time \times membrane surface area)). Concentration dependence tests using IONP@SDS in (a) FO mode and (b) PRO mode.

coating-dependent tests were performed using an identical IONPs concentration (900 ppm) with various organic stabilizers, including SDS, CTAB, and PEG. As shown in Fig. 4, the water fluxes were 0.42 , 0.14 , and $0.32 \text{ L/m}^2\text{-h}$ for IONP@SDS, IONP@CTAB, and IONP@PEG, respectively, in FO mode, and 0.60 , 0.56 , and $0.65 \text{ L/m}^2\text{-h}$ for IONP@SDS, IONP@CTAB, and IONP@PEG, respectively, in PRO mode. For the tested organic coatings, IONPs performance was similar in PRO mode. In contrast, performance varied considerably in FO mode, depending on the coating type. To create effective osmotic pressure in FO mode, draw solutes in the bulk solution should diffuse to the end of the support layer (i.e., toward the active layer). A thin organic coating layer of IONPs (e.g., SDS) is better for diffusion than a thick layer (e.g., PEG). Also, positively charged IONP@CTAB showed a considerably lower water flux than negatively charged IONPs (IONP@SDS and IONP@PEG). The membrane, composed of a polyamide thin film with polysulfone supports, has a negative surface charge³¹. We speculate that oppositely charged IONPs (e.g., IONP@CTAB) are difficult to transport/diffuse in thick support layer(s), resulting in considerable ICP.

Flux enhancement

To improve the draw solute performance, we explored the use of hollow IONPs (HNPs) as draw solutes and oscillating magnetic field. The inners of core IONPs were hollowed to increase the number concentration of NPs (osmotic pressure) for the same mass concentration. With respect to the hollow nanoparticles, the thickness of shell is important factor to increase the number

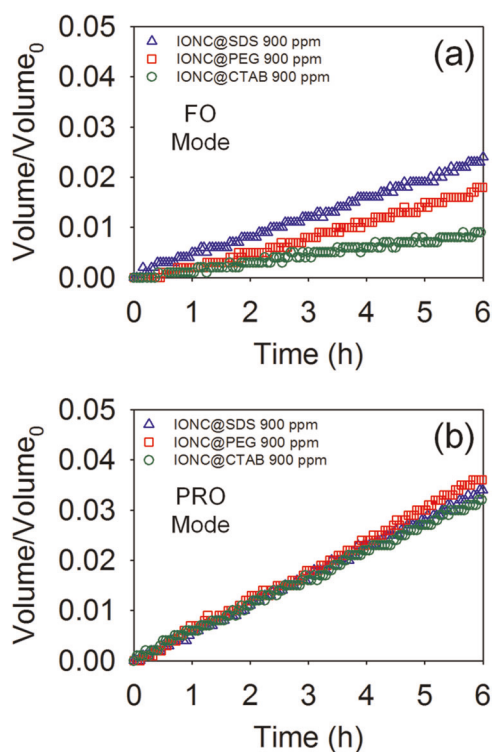


Fig. 4 Draw solute performances of synthesized NPs in osmotic pressure driven membrane processes (FO and PRO modes). Water fluxes were measured by time dependent total volume increase (V/V_0) with 0.95 cm^2 of effective membrane surface area (water flux = Increased volume/(time \times membrane surface area)). Organic coating dependence tests using IONP@SDS, IONP@PEG, and IONP@CTAB in (a) FO mode and (b) PRO mode.

concentration of NPs under the same mass concentration. As shown in Fig. 1b, the thickness of HNPs is under 2 nm and we have calculated and presented the increase osmotic pressure as a function of shell thickness in Supplementary Fig. 2.

High colloidal stability is critical to draw solute performance by preventing aggregation and membrane blocking. Colloidal stabilities of both IONPs and HNPs were investigated by measuring the critical coagulation concentration (CCC). Both HNP@SDS and IONP@SDS had similar colloidal stabilities; CCC values were 175 and 159 mM in NaCl for HNP@SDS and IONP@SDS, respectively (Fig. 5a). For the same mass concentration (900 ppm), water flux was enhanced using HNPs as they increased the number concentration (Fig. 5b). Comparatively, the water fluxes were 0.53 and $1.11 \text{ L/m}^2\text{-h}$ for HNP@SDS in FO and PRO modes, respectively.

We next demonstrated further improvement of the CP profile when organic coated IONPs were used as draw solutes and exposed to an external magnetic field. The magnetic properties of IONPs were characterized by SQUID analysis (Supplementary Fig. 3). Hysteresis loops showed IONPs are superparamagnetic at room temperature (300 K) with nearly zero remanence. The average coercivity and exchange bias were 11.6 Oe and -0.23 Oe , respectively at 300 K . We applied a magnetic field using the stator of AC motor, as illustrated in Fig. 6a. This stator is a part of motor (1125 RPM) of tractor (730 , John Deere). The stator coils produce an oscillating magnetic field; field strength is proportional to applied AC^{32,33}. Here, we applied 10 times lower current (880 mA) than original current of tractor battery. Magnetic field-dependence tests were implemented using 1800 ppm of IONP@SDS as a draw solute in both FO and PRO modes. As shown in Fig. 6b, water flux was increased by 23% in FO mode and 80% in PRO mode upon application of the magnetic field. We hypothesize that the magnetic field has a direct effect on ICP via physically enhancing diffusion of

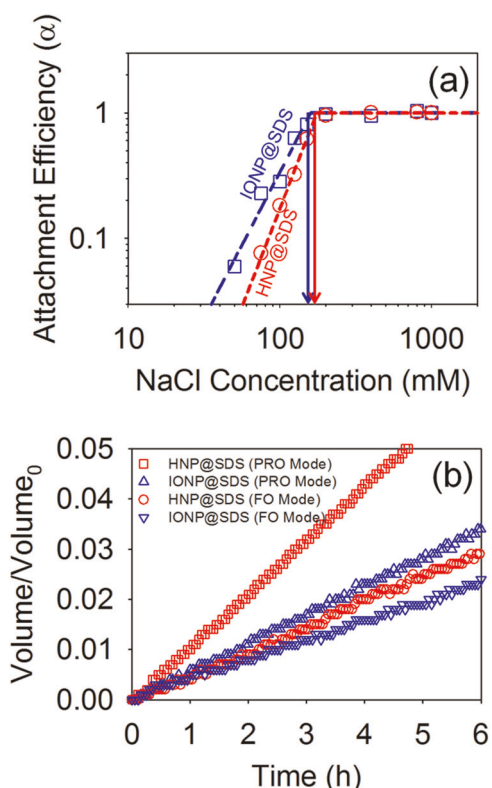


Fig. 5 Draw solute performance and stability of HNPs. (a) Attachment efficiency of IONP@SDS (blue) and HNP@SDS (red) as a function of NaCl concentration. (b) Draw solute performances of synthesized IONP@SDS and HNP@SDS in osmotic pressure driven membrane processes (FO and PRO modes). Initial particle concentration was 900 ppm. Water fluxes were measured by time dependent total volume increase (V/V_0) (water flux = Increased volume/(time \times membrane surface area)).

the draw solute. Oscillating magnetic field control and optimization, including direction and strength, are also important factor to be considered for scaled applications, which was beyond the scope of this initial study. To our knowledge this is the first case that stable magnetic particles were demonstrated to increase flux via applied magnetic field, with no loss in performance due to nano aggregation/membrane blocking, for osmotic driven processes, opening the door for considerable future research.

METHODS

Materials

Iron oxy hydroxide (FeOOH), oleic acid (OA, technical grade, 90%), 1-octadecene (ODE, technical grade, 90%), cetyltrimethylammonium bromide (CTAB, 95%), sodium dodecyl sulfate (SDS, 99%), poly (ethylene glycol) (PEG, Mw = 5000), trioctylphosphine oxide (TOPO, technical grade 90%), ethanol (99.9%), acetone (99.5%), and hexane (98.5%) were purchased from Sigma-Aldrich.

Synthesis of IONPs

IONPs were synthesized by iron oxyhydroxide decomposition at 320 °C^{20,24}. FeOOH (2 mmol) with OA (6 mmol) were used in the ODE (5 g) as a solvent. Detailed information about the synthesis and purification processes for NPs was given in our previous research and other sources^{20,24}.

Synthesis of hollow IONPs (HNPs)

Synthesized IONPs were hollowed out at 300 °C using technical grade TOPO as an acid etching agent²⁵. IONPs in hexane (particular

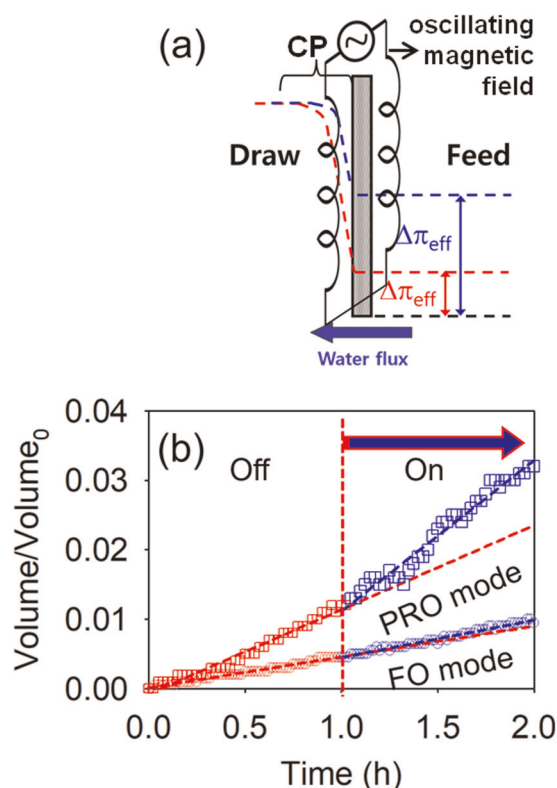


Fig. 6 Flux enhancement by oscillating magnetic field. (a) Schematic diagrams of oscillating magnetic field for improvement of the concentration polarization (CP) profile of IONPs. Here $\Delta\pi_{eff}$ is effective osmotic pressure difference between draw and feed solution. (b) Total volume increase (V/V_0) as a function of time before and after oscillating magnetic field control in FO and PRO modes. Initial particle concentration was 1800 ppm using 12 nm IONP@SDS.

concentration was 7.8×10^{18} particles) with TOPO (9 g) were used in the 3 g of ODE as a solvent. The resulting HNPs were purified using ethanol (20 mL) and acetone (25 mL), and centrifuged at 8000 rpm for 15 min at 5 °C. The purification processes were repeated six times. The purified NPs were dispersed and stored in hexane.

Organic coating

Synthesized IONPs were organically functionalized by ligand exchange using PEG, and by ligand encapsulation using SDS and CTAB^{9,23}. Detailed information about the organic functionalization protocol and washing processes is given in elsewhere^{24,26,27,34}. Resulting phase transferred IONPs were concentrated under gentle vacuum.

Transmission electron microscope (TEM)

For over a thousand synthesized NPs, the size and size distributions were measured using a transmission electron microscope (TEM, Tecnai G2 Spirit, FEI) and Image Pro Plus 6.0 software (Media Cybernetics, USA)³⁵.

Hydrodynamic diameter and zeta potential

The hydrodynamic diameters and zeta potential of aqueous phase IONPs were determined by a dynamic light scattering (DLS) method (Malvern, Zetasizer Nano ZS, ZEN3600) at pH 7 and 22 °C.

Colloidal stability

The colloidal stability of NPs was evaluated via critical coagulation concentration (CCC) measurement using DLS. The protocol for CCC measurements was given elsewhere^{36–38}.

Osmotic pressure driven membrane system

A diffusion/osmosis apparatus having U-shaped tube (0.95 cm² of effective surface area) was used as the osmotic pressure driven membrane system, with a Porifera membrane (A flat-sheet form, Hayward, CA, USA). Detailed characteristics about membrane can be found in other studies^{39,40}. Engineered superparamagnetic NPs were used as draw solutes, with 10 mL of initial draw solution volume. DI water (>18.2 MΩ-cm resistivity, Milli-Q, Millipore Corp) was used as a feed solution and was connected to a digital balance (ML 1502E, Mettler Toledo). We measure the volume increase of feed solution every 3 min, and water flux was calculated considering the effective membrane surface area (water flux = Increased volume/time × membrane surface area). All experiments were conducted at room temperature.

Magnetic field system

The outside stator of an alternating current (AC) motor (Delco, 1103021, 24 volt) were used as a field coil.

X-ray diffraction (XRD)

XRD patterns of synthesized NPs were measured using a powder diffractometer (Bruker d8 Advance X-ray Diffractometer) with Cu Kα radiation (1.54 Å).

Superconducting quantum interference device (SQUID)

Magnetization hysteresis loops were obtained using a superconducting quantum interference device (SQUID) magnetometer (Quantum Design MPMS 5XL SQUID) at 300 K.

DATA AVAILABILITY

The authors declare that [the/all other] data supporting the findings of this study are available within the paper [and its supplementary information files].

Received: 2 August 2019; Accepted: 7 February 2020;

Published online: 24 March 2020

REFERENCES

- Lutchmiah, K., Verliefe, A., Roest, K., Rietveld, L. C. & Cornelissen, E. R. Forward osmosis for application in wastewater treatment: a review. *Water Res.* **58**, 179–197 (2014).
- Altaee, A., Zaragoza, G., Drioli, E. & Zhou, J. Evaluation the potential and energy efficiency of dual stage pressure retarded osmosis process. *Appl. Energy* **199**, 359–369 (2017).
- McCutcheon, J. R., McGinnis, R. L. & Elimelech, M. A novel ammonia-carbon dioxide forward (direct) osmosis desalination process. *Desalination* **174**, 1–11 (2005).
- Phillip, W. A., Yong, J. S. & Elimelech, M. Reverse draw solute permeation in forward osmosis: modeling and experiments. *Environ. Sci. Technol.* **44**, 5170–5176 (2010).
- Murad, E. & Cashion, J. in *Mössbauer Spectroscopy of Environmental Materials and their Industrial Utilization* (Springer Science & Business Media, 2004) <https://doi.org/10.1007/978-1-4419-9040-2>.
- Arami, H., Khandhar, A., Liggitt, D. & Krishnan, K. M. In vivo delivery, pharmacokinetics, biodistribution and toxicity of iron oxide nanoparticles. *Chem. Soc. Rev.* **44**, 8576–8607 (2015).
- Yang, H. M., Seo, B. K., Lee, K. W. & Moon, J. K. Hyperbranched polyglycerol-coated manetic nanoparticles as draw solute in forward osmosis. *Asian J. Chem.* **26**, 4031–4034 (2014).
- Ling, M. M. & Chung, T. S. Desalination process using super hydrophilic nanoparticles via forward osmosis integrated with ultrafiltration regeneration. *Desalination* **278**, 194–202 (2011).
- Sperling, R. A. & Parak, W. Surface modification, functionalization and bioconjugation of colloidal inorganic nanoparticles. *Philos. Trans. R. Soc. Lond. A* **368**, 1333–1383 (2010).
- Dey, P. & Izake, E. L. Magnetic nanoparticles boosting the osmotic efficiency of a polymeric FO draw agent: effect of polymer conformation. *Desalination* **373**, 79–85 (2015).
- Ling, M. M. & Chung, T. S. Surface-dissociated nanoparticle draw solutions in forward osmosis and the regeneration in an integrated electric field and nano-filtration system. *Ind. Eng. Chem. Res.* **51**, 15463–15471 (2012).

- Yang, H.-M. et al. Succinate functionalization of hyperbranched polyglycerol-coated magnetic nanoparticles as a draw solute during forward osmosis. *J. Nanosci. Nanotechnol.* **15**, 8279–8284 (2015).
- Bai, H. W., Liu, Z. Y. & Sun, D. D. Highly water soluble and recovered dextran coated Fe₃O₄ magnetic nanoparticles for brackish water desalination. *Sep. Purif. Technol.* **81**, 392–399 (2011).
- Na, Y., Yang, S. & Le, S. Evaluation of citrate-coated magnetic nanoparticles as draw solute for forward osmosis. *Desalination* **347**, 34–42 (2014).
- Ge, Q. C., Su, J. C., Chung, T. S. & Amy, G. Hydrophilic superparamagnetic nanoparticles: synthesis, characterization, and performance in forward osmosis processes. *Ind. Eng. Chem. Res.* **50**, 382–388 (2011).
- Ge, Q., Su, J., Chung, T.-S. & Amy, G. Hydrophilic superparamagnetic nanoparticles: synthesis, characterization, and performance in forward osmosis processes. *Ind. Eng. Chem. Res.* **50**, 382–388 (2010).
- Park, S. Y., Ahn, H.-W., Chung, J. W. & Kwak, S.-Y. Magnetic core-hydrophilic shell nanosphere as stability-enhanced draw solute for forward osmosis (FO) application. *Desalination* **397**, 22–29 (2016).
- Guizani, M., Maeda, T., Ito, R. & Funamizu, N. Synthesis and characterization of magnetic nanoparticles as a candidate draw solution for forward osmosis. *J. Water Environ. Technol.* **16**, 63–71 (2018).
- Park, J. et al. Ultra-large-scale syntheses of monodisperse nanocrystals. *Nat. Mater.* **3**, 891–895 (2004).
- William, W. Y., Falkner, J. C., Yavuz, C. T. & Colvin, V. L. Synthesis of monodisperse iron oxide nanocrystals by thermal decomposition of iron carboxylate salts. *Chem. Commun.* **20**, 2306–2307 (2004).
- Kang, Y. S., Risbud, S., Rabolt, J. F. & Stroeve, P. Synthesis and characterization of nanometer-size Fe₃O₄ and γ-Fe₂O₃ particles. *Chem. Mater.* **8**, 2209–2211 (1996).
- Lopez Perez, J., Lopez Quintela, M., Mira, J., Rivas, J. & Charles, S. Advances in the preparation of magnetic nanoparticles by the microemulsion method. *J. Phys. Chem. B* **101**, 8045–8047 (1997).
- Prakash, A. et al. Bilayers as phase transfer agents for nanocrystals prepared in nonpolar solvents. *ACS nano* **3**, 2139–2146 (2009).
- Kim, C., Lee, S. S., Lafferty, B. J., Giammar, D. & Fortner, J. Engineered superparamagnetic nanomaterials for arsenic (V) and chromium (VI) sorption and separation: quantifying the role of organic surface coatings. *Environ. Sci.* **5**, 556–563 (2018).
- An, K. et al. Synthesis of uniform hollow oxide nanoparticles through nanoscale acid etching. *Nano Lett.* **8**, 4252–4258 (2008).
- Lee, S. S. et al. Surface functionalized manganese ferrite nanocrystals for enhanced uranium sorption and separation in water. *J. Mater. Chem. A* **3**, 21930–21939 (2015).
- Kim, C. et al. Surface-optimized core-shell nanocomposites (Fe₃O₄@MnxFeyO₄) for ultra-high uranium sorption and low-field separation in water. *Environ. Sci.* **5**, 2252–2256 (2018).
- Hotze, E. M., Phenrat, T. & Lowry, G. V. Nanoparticle aggregation: challenges to understanding transport and reactivity in the environment. *J. Environ. Qual.* **39**, 1909–1924 (2010).
- Phenrat, T. et al. Stabilization of aqueous nanoscale zerovalent iron dispersions by anionic polyelectrolytes: adsorbed anionic polyelectrolyte layer properties and their effect on aggregation and sedimentation. *J. Nanopart. Res.* **10**, 795–814 (2008).
- Cath, T. Y., Childress, A. E. & Elimelech, M. Forward osmosis: principles, applications, and recent developments. *J. Membr. Sci.* **281**, 70–87 (2006).
- Blandin, G., Vervoort, H., Le-Clech, P. & Verliefe, A. R. Fouling and cleaning of high permeability forward osmosis membranes. *J. Water Process Eng.* **9**, 161–169 (2016).
- Tesla, N. in *Electro-magnetic motor* (Google Patents, 1888).
- Phillips, K. P. Current-source converter for ac motor drives. *IEEE Trans. Industry Appl.* **6**, 679–683 (1972).
- Lee, S. S. et al. Engineered manganese oxide nanocrystals for enhanced uranyl sorption and separation. *Environ. Sci.* **2**, 500–508 (2015).
- Vigneau, E., Loisel, C., Devaux, M. & Cantoni, P. Number of particles for the determination of size distribution from microscopic images. *Powder Technol.* **107**, 243–250 (2000).
- Mylon, S. E., Chen, K. L. & Elimelech, M. Influence of natural organic matter and ionic composition on the kinetics and structure of hematite colloid aggregation: Implications to iron depletion in estuaries. *Langmuir* **20**, 9000–9006 (2004).
- Holthoff, H., Egelhaaf, S. U., Borkovec, M., Schurtenberger, P. & Sticher, H. Coagulation rate measurements of colloidal particles by simultaneous static and dynamic light scattering. *Langmuir* **12**, 5541–5549 (1996).
- Chen, K. L., Mylon, S. E. & Elimelech, M. Aggregation kinetics of alginate-coated hematite nanoparticles in monovalent and divalent electrolytes. *Environ. Sci. Technol.* **40**, 1516–1523 (2006).

39. Nasr, P. & Sewilam, H. Investigating fertilizer drawn forward osmosis process for groundwater desalination for irrigation in Egypt. *Desalination Water Treat.* **57**, 26932–26942 (2016).
40. Choi, B. G., Zhan, M., Shin, K., Lee, S. & Hong, S. Pilot-scale evaluation of FO-RO osmotic dilution process for treating wastewater from coal-fired power plant integrated with seawater desalination. *J. Membr. Sci.* **540**, 78–87 (2017).

ACKNOWLEDGEMENTS

This work was supported by U.S. Army Corps of Engineers (W912HZ-13-2-0009-P00001), the US National Science Foundation (CBET 1437820), and the NSF Nanosystems Engineering Research Center for Nanotechnology-Enabled Water Treatment (ERC-1449500). TEM, XRD, ICP-OES, and DLS were provided by the Nano Research Facility (NRF) and Institute of Materials Science and Engineering at Washington University in St. Louis. The authors acknowledge Professor James C. Ballard for reviewing the paper.

AUTHOR CONTRIBUTIONS

C.K. carried out the project, and interpreted data, and wrote paper. J.L. provided lab experiments data, material analysis, and nanomaterial synthesis. D.S. contributed on the preparation of nano materials. J.D.F. supervised development of work, helped in data interpretation and paper preparation.

COMPETING INTERESTS

The authors declare no competing interests.

ADDITIONAL INFORMATION

Supplementary information is available for this paper at <https://doi.org/10.1038/s41545-020-0055-9>.

Correspondence and requests for materials should be addressed to J.D.F.

Reprints and permission information is available at <http://www.nature.com/reprints>

Publisher's note Springer Nature remains neutral with regard to jurisdictional claims in published maps and institutional affiliations.



Open Access This article is licensed under a Creative Commons Attribution 4.0 International License, which permits use, sharing, adaptation, distribution and reproduction in any medium or format, as long as you give appropriate credit to the original author(s) and the source, provide a link to the Creative Commons license, and indicate if changes were made. The images or other third party material in this article are included in the article's Creative Commons license, unless indicated otherwise in a credit line to the material. If material is not included in the article's Creative Commons license and your intended use is not permitted by statutory regulation or exceeds the permitted use, you will need to obtain permission directly from the copyright holder. To view a copy of this license, visit <http://creativecommons.org/licenses/by/4.0/>.

© The Author(s) 2020